Effects of microstructure and crystallography on crack path and intrinsic resistance to shear-mode fatigue crack growth

J. Pokluda
Faculty of Mechanical Engineering, Brno University of Technology, Technická 2, CZ-61669 Brno, Czech Republic
Central European Institute of Technology (CEITEC), Brno University of Technology, Technická 3058/10, CZ-61600 Brno, Czech Republic
pokluda@fme.vutbr.cz

T. Vojtek
Erich Schmid Institute of Materials Science, Austrian Academy of Sciences, Jahnstr. 12, A-8700 Leoben, Austria
Central European Institute of Technology (CEITEC), Brno University of Technology, Technická 3058/10, CZ-61600 Brno, Czech Republic
tomas.vojtek@ceitec.vutbr.cz

A. Hohenwarter
Department of Materials Physics, Montanuniversität Leoben, Jahnstr. 12, A-8700 Leoben, Austria
anton.hohenwarter@unileoben.ac.at

R. Pippan
Erich Schmid Institute of Materials Science, Austrian Academy of Sciences, Jahnstr. 12, A-8700 Leoben, Austria
reinhard.pippan@oeaw.ac.at

ABSTRACT. The paper focuses on the effective resistance and the near-threshold growth mechanisms in the ferritic-pearlitic and the pure pearlitic steel. The influence of microstructure on the shear-mode fatigue crack growth is divided here into two factors: the crystal lattice type and the presence of different phases. Experiments were done on ferritic-pearlitic steel and pearlitic steel using three different specimens, for which the effective mode II and mode III threshold values were measured and fracture surfaces were reconstructed in three dimensions using stereophotogrammetry in scanning electron microscope. The ferritic-pearlitic and pearlitic steels showed a much different behaviour of modes II and III cracks than that of the ARMCO iron. Both the deflection angle and the mode II threshold were much higher and comparable to the austenitic steel. Mechanism of shear-mode crack behaviour in the ARMCO iron, titanium and nickel were described by the model of emission of dislocations from the crack tip under a dominant mode II loading. In other tested materials the cracks propagated under a dominance of the local mode I. In the ferritic-pearlitic and pearlitic steels, the reason for such behaviour was the presence of the secondary-phase particles (cementite lamellas), unlike in the previously austenitic steel, where the fcc structure and the low stacking fault energy were the main factors. A criterion for mode I deflection from the mode II crack-tip loading, which uses values of the effective mode I and mode II thresholds, was in agreement with fractographical observations.

KEYWORDS. mode II and mode III cracks, ferritic-pearlitic steel, pearlitic steel, micromechanism, mode I branching

INTRODUCTION

Observation of crack paths on a microscopic level enables us to reveal local loading modes at the crack tip under various kinds of remote loading. In the recent works [1 – 3], such an analysis was done for pure mode II and mode III loading which led to a proposal of relationship for intrinsic resistance to crack propagation under pure mode II near- threshold loading and a verification of mode-I-branching criterion. This paper broadens the experimental data by presenting results obtained for steels with two different microstructures, which are compared with other previously tested materials. Identification of the effect of microstructure of multiphase materials contributes to the research of shear-mode crack growth micromechanisms.

The influence of microstructure on the shear-mode fatigue crack growth is divided here into two factors: the crystal lattice type and the presence of different phases. The first factor was previously studied on four single-phase metals, namely the ARMCO iron, titanium, nickel and stainless steel [3]. Crystal lattices of the first three materials have sufficient numbers of slip systems that enable the crack propagation described by the emission dislocation model [2]. In this model, the crack growth mechanism is realized as cyclic blunting and re-sharpening of the crack tip, during which (shielding) dislocations are emitted from the crack tip and some of them come back to the tip during the unloading phase. Emission of dislocations from the tip of a mode II loaded crack is easy when conveniently oriented slip systems are available.

Results from the first three materials show a good correlation between the availability of slip planes and the measured angles of deflected remote mode II cracks with respect to the original crack plane. In pure ferrite (ARMCO iron) the dense set of slip planes of the bcc lattice enables a selection of the slip systems oriented almost parallel to the applied shear stress. This is probably the reason why the shear cracks in this material propagate almost coplanarly (small deflection angle) and the intrinsic mode II threshold is the lowest one of all tested materials. In the hcp lattice of titanium there are higher angles between the slip planes than in the bcc structure and some of the slip systems are harder to activate which results in a bigger deflection angle and a higher intrinsic mode II threshold. The fcc lattice of nickel has even higher angles between the (111) slip planes, which is in agreement with a big measured mean deflection angle of the remote mode II loaded cracks. The mode II intrinsic threshold was also high here, which can be related to a low Schmid factor in the highly deflected planes. This good agreement between the deflection angles and the values of thresholds (see also Tab. 1) is reflected by a successful use of a simple physical-based relationship for intrinsic mode II threshold, Eq. (1), for single-phase metals. This formula takes into account only the strength of interatomic bonds, the dislocation mobility and the crystallography:

$$\Delta K_{\mathrm{IIeff,th}} = G b^{1/2} / n_{\alpha} , \tag{1}$$

where

$$n_{\alpha} = \frac{1}{2}\cos\frac{\alpha_{\mathrm{IIm}}}{2}\left(3\cos\alpha_{\mathrm{IIm}} - 1\right),$$

G is the shear modulus, b is the magnitude of Burgers vector and a_{IIm} is the mean deflection angle of the crack front from the plane of the maximum shear stress [3]. Let us also mention that the effective mode I threshold can be predicted using the formula

$$\Delta K_{\mathrm{Ieff,th}} = 0.75\ E\ b^{1/2}. \tag{2}$$

The other studied material was the stainless steel. The stainless steel (X5CrNi18-10) had the fcc lattice but, apart from nickel, it has a low stacking-fault energy. The presence of stacking faults prevents dislocations from cross slip and limits their manoeuvrability significantly. Therefore, not only the deflection angle is bigger than that in nickel but also the fracture surface morphology was completely different. Both mode II and mode III cracks propagated in pure mode I and the fracture surfaces contained no crystallographic facets [1]. Therefore, the effective mode II threshold was controlled by

Eq. (2). It was suggested that in this material a different crack growth mechanism was predominant [2]. In the model of this mechanism the crack propagates by absorption of antishielding dislocations by the crack tip and when dislocations come very near to the crack tip (a few lattice spacings) a decohesion occurs. This mechanism is efficient only when the crack kinks to the opening mode. The shear mechanism (emission of dislocations) is hard to realize here which results in the dominance of the decohesion mechanism.
This article focuses on the effective resistance and the near-threshold growth mechanisms in the ferritic-pearlitic and the pure pearlitic steel. Moreover, a simple criterion for mode I deflection from the mode II crack-tip loading will also be discussed with respect to the fractography observations [3]. A linear elastic fracture mechanics condition for mode I deflection is [e. g. 4]:

$$\Delta k_{\mathrm{I}} = 1.15\,\Delta K_{\mathrm{IIeff,th}} \geq \Delta K_{\mathrm{Ieff,th}}\,, \tag{3}$$

where Δk_{I} is the local stress intensity factor for an elementary mode I branch. Evaluation of this criterion is in a good agreement with the observed deflection angles a_{II} and the related mode mixities, summarized in Tab. 2. Mode mixities can be calculated according to Eq. (4) using local stress intensity factors Δk_{I} and Δk_{II} [3]:

$$\frac{\Delta k_{\mathrm{IIeff}}}{\Delta k_{\mathrm{Ieff}}} = \frac{3\cos\alpha_{\mathrm{II}} - 1}{3\sin\alpha_{\mathrm{II}}} \tag{4}$$

EXPERIMENTS

Experiments were done on ferritic-pearlitc steel (ISO C60E4, 0.45 w% C) and a pearlitic steel for rails (R260) using three different specimens: the CTS specimens for pure mode II loading, the cylindrical specimens with circumferential crack loaded in torsion for pure mode III and cylindrical specimens with circumferential crack loaded in a special device by pure shear for a combined loading of modes II, III and II + III. A more detailed description of the specimens can be found in [2] and the microstructure of both investigated steels is depicted in Fig. 1. Precracks were made at the notch roots of the specimens by cyclic compressive loading. This procedure eliminates extrinsic shielding (friction and residual stress) at the beginning of the shear-mode experiments and enables measurements of effective values of the stress intensity factor range at the threshold for pure modes II and III loading [2, 3]. After the experiments the specimens were fractured in mode I. Threshold values were determined directly from the dependence of crack growth rate on stress intensity factor range.

	Measured angles [°]		Effective thresholds [MPam$^{1/2}$]		
	Deflection a Mode II	Twisting β Mode III	Mode II calculated	Mode II measured	Mode III measured
ARMCO iron	19 ± 13	16 ± 12	1.4 *	1.5 a)	2.6 a)
Titanium	39 ± 21	36 ± 20	1.7 *	1.7 a)	2.8 a)
Nickel	52 ± 24	36 ± 22	2.4 *, 3.1 **	2.9 a)	4.3 a)
Ferritic-pearlitic steel	50 ± 14	31 ± 18	3.2 *, 2.5 **	2.7	4.4
Pearlitic steel	60 ± 8	41 ± 18	2.5 **	2.7	4.5
Stainless steel	67 ± 5	39 ± 16	2.5 **	2.5 a)	4.2 a)

a) [3], * Eq. (1), ** Eq. (2)

Table 1: Summary of the experimentally obtained values of deflection angles of mode II loaded cracks, twist angles of mode III loaded cracks and the effective thresholds in mode II and mode III for 6 metallic materials. Effective mode II thresholds calculated using Eq. (1) is shown for comparison. For materials with a large local mode I component the values according to Eq. (2) are shown.

Fracture surfaces were reconstructed in 3D using the stereophotogrammetry in the scanning electron microscope (SEM) [5]. Quantification of the 3D data was done by a profile analysis – see Figs. 2 – 5. The coordinate l passes along the line

from the left to the right and the topological profiles were determined by the vertical coordinate z. These profiles were used for a measurement of angles corresponding to the average crack deviation from the plane of the maximum shear stress. The profiles running parallel to the shear direction provide angles a of crack deflection, while those of the perpendicular direction indicate angles β of the crack twisting.
Figs. 2 – 5 show fracture surfaces with profiles running along the coordinate l defined by the white arrow in figures. This coordinate and the white arrows are parallel to the applied shear direction in all figures. The height is given by the coordinate z, which also corresponds to the colour codes. One can compare the morphologies with those for ARMCO iron, titanium, nickel and stainless steel published in [1 – 3]. Tab. 1 summarizes the measured and calculated data for all materials tested up to now. The first two columns show mean values and standard deviations of measured angles between a deflected or twisted crack and the original crack plane. Angles close to 70° for mode II and close to 45° for mode III indicate local mode I propagation. The third column shows values of intrinsic thresholds calculated according to Eq. (1) for materials with predominant mode II local loading (lower deflection and twist angles) and according to Eq. (2) for those exhibiting almost pure local mode I crack growth. Experimentally measured mode II and mode III effective thresholds are presented in the last two columns.

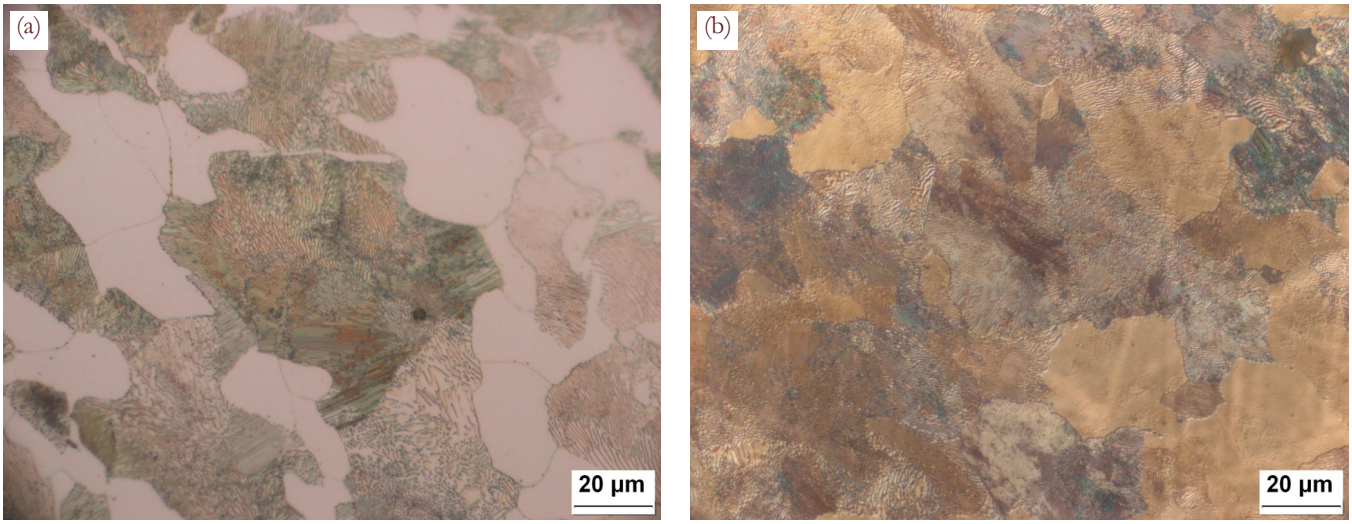

Figure 1: Microstructure of the investigated ferritic-pearlitic steel (a) and pearlitc steel (b).

DISCUSSION

The fully pearlitic steel showed a very different behaviour of modes II and III cracks than in the ARMCO iron. Both the deflection angle and the mode II threshold were much higher and comparable to the austenitic steel (see Tab. 1). In pearlite, the cementite lamellae represent a strong barrier for dislocations. Therefore, the deformation mechanism is limited to the small volume of ferrite between the lamellae (in the near-threshold regime). The barriers have to be bypassed, which may cause a kink of the crack with high angles. In pearlite, areas of micro-cleavage at ferrite-cementite interfaces and crack cutting across cementite lamellae were observed for mode I fatigue crack growth [6, 7]. It is expected that a similar mechanism takes place also in the case of cracks loaded by modes II and III. The above mentioned mechanisms explain the observed high deflections of the remote mode II cracks towards a nearly pure opening mode I in this material. Although the ferritic-pearlitic steel contained approximately the same portion of ferrite and pearlite, the deflection angle was only slightly smaller than that in the fully pearlitic steel and the value of the effective mode II threshold was fully comparable. This indicates that after the local mode I growth is triggered in the pearlitic grain, the crack propagation continues with a large component of mode I also in the rest of the material.
Thus, the presence of the pearlitic phase makes a relatively big difference in nature of the shear-mode fatigue crack growth when compared with that of pure ferrite. In all the stainless, ferritic-pearlitic and pearlitic steels the crack immediately deflects to the opening mode I. Therefore, Eq. (2) should be used for prediction of their mode II threshold values. In the ferritic-pearlitic and pearlitic steels, the reason for such behaviour is the presence of the secondary-phase particles (cementite lamellas). In the austenitic steel, on the other hand, the fcc structure and the low stacking fault energy are the main factors.

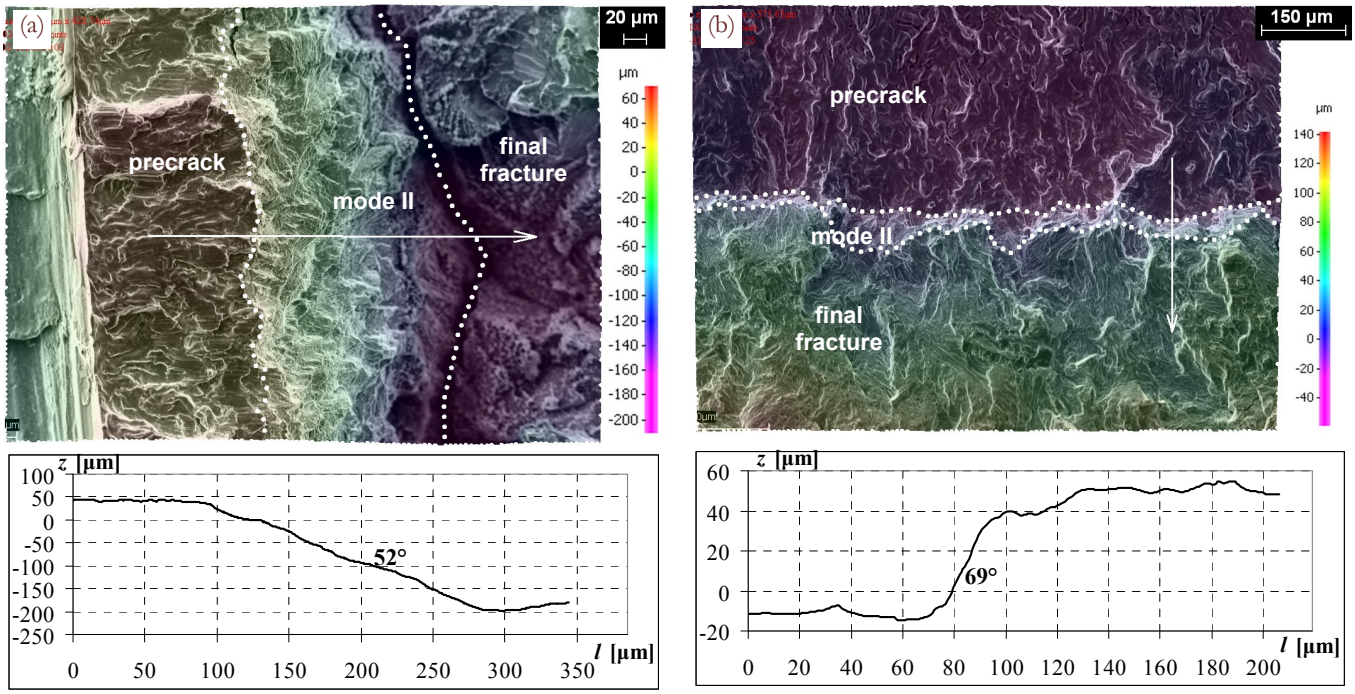

Figure 2: Mode II in ferritic-pearlitic steel, cylindrical shear specimen (a), compact-tension shear specimen (b). The white arrow defines the profile showed below and is parallel to the applied shear direction.

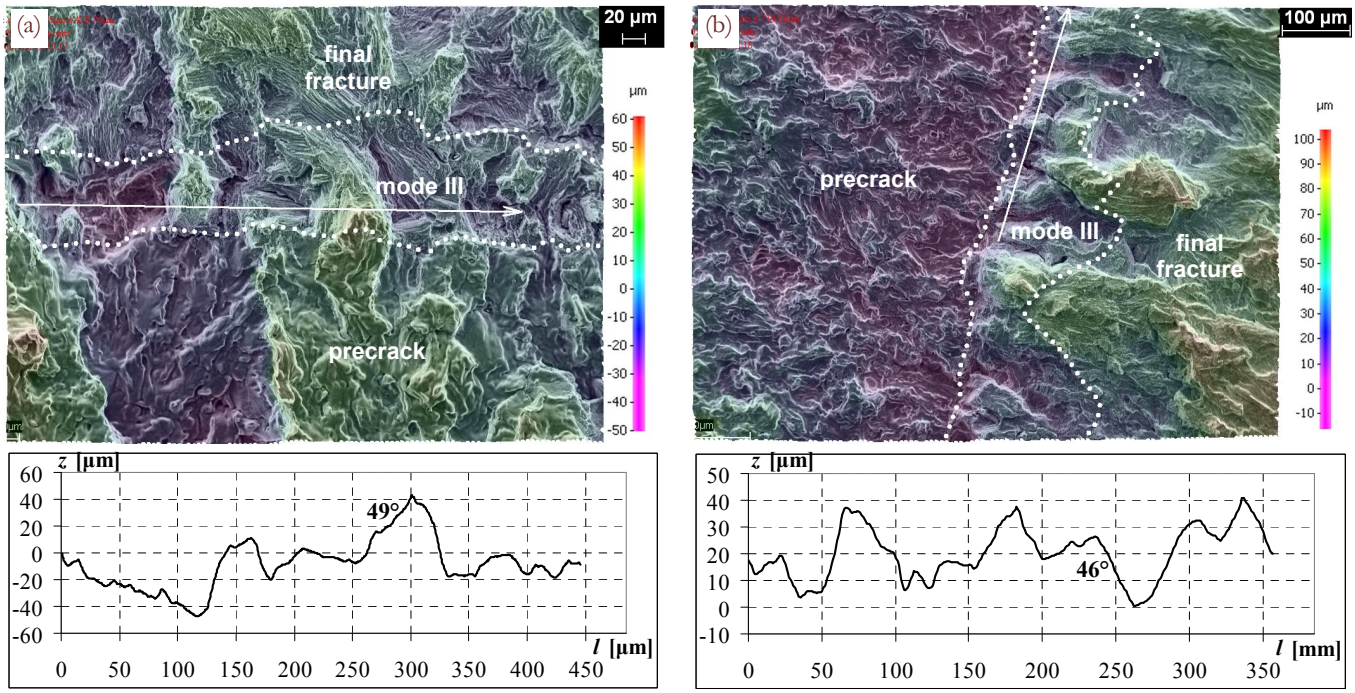

Figure 3: Mode III in ferritic-pearlitic steel, cylindrical shear specimen (a), torsion specimen (b). The white arrow defines the profile showed below and is parallel to the applied shear direction.

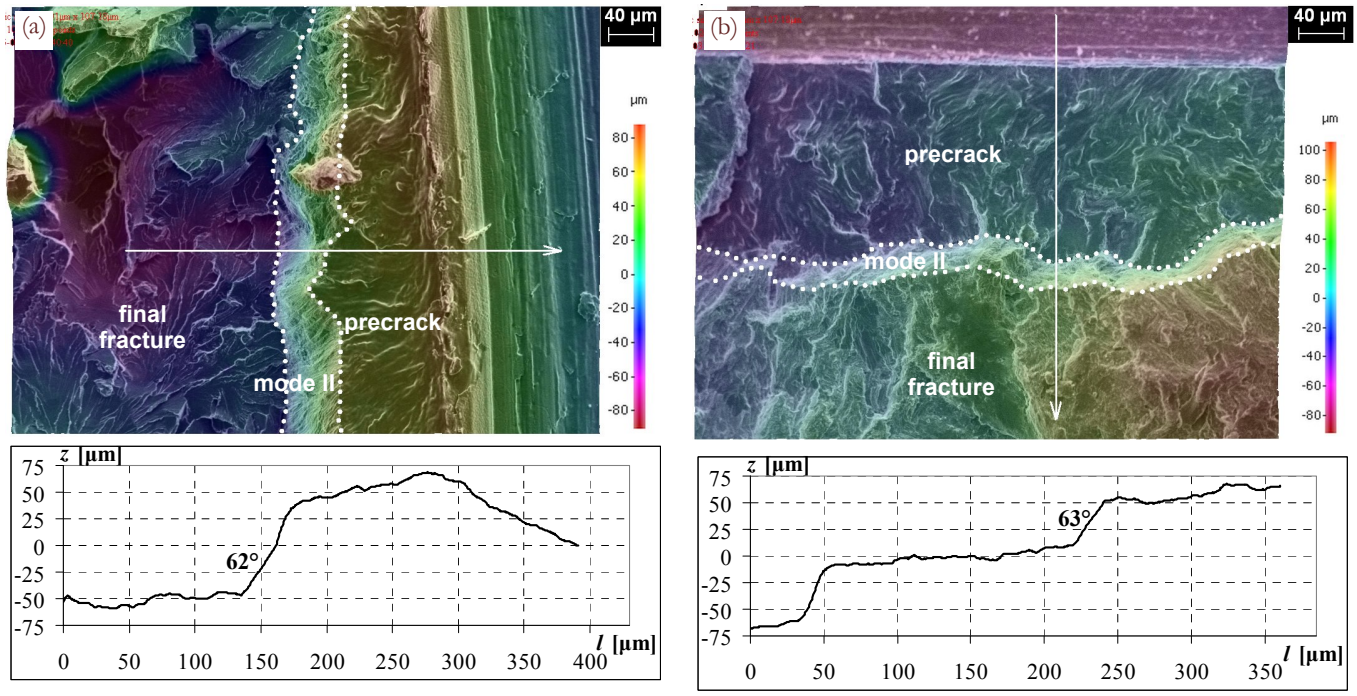

Figure 4: Mode II in pearlitic steel, cylindrical shear specimen (a), compact-tension shear specimen (b). The white arrow defines the profile showed below and is parallel to the applied shear direction.

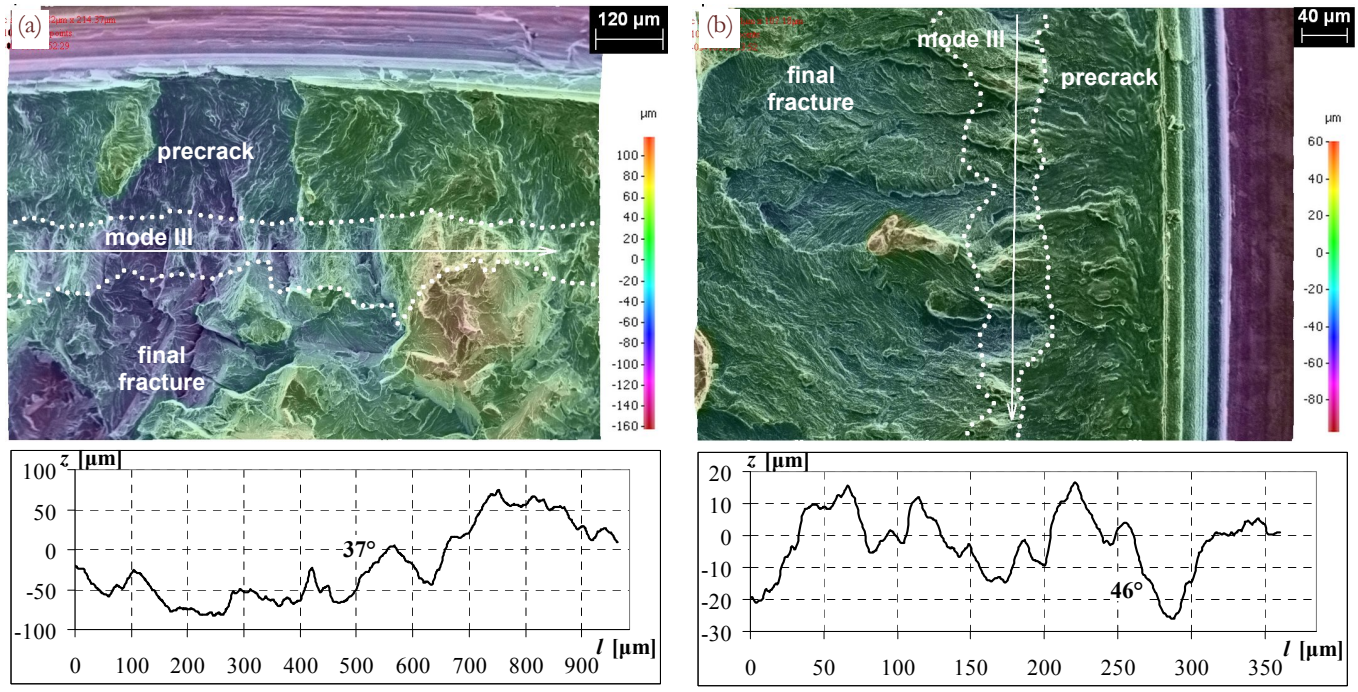

Figure 5: Mode III in pearlitic steel, cylindrical shear specimen (a), torsion specimen (b). The white arrow defines the profile showed below and is parallel to the applied shear direction.

A fulfilment of the deflection (branching) criterion (3) is demonstrated in Tab. 2. The criterion was not fulfilled for the ARMCO iron where no mode I branching was observed (deflection $a_{II} \approx 19°$). Medium-sized deflection angles in titanium correspond to approximately equal sides of the criterion. For other materials the criterion was fulfilled and considerable deflections towards local mode I were observed to various levels. For nickel and ferritic-pearlitic steels, both the deflection angles and the mode mixities revealed an almost balanced contribution of local modes I and II. Therefore, values of the mode II threshold calculated using both Eqs. (1) and (2) are displayed in Tab. 1. On the other hand, almost pure local mode I loading was detected in pearlitic and stainless steel. For these materials, consequently, only threshold values calculated according to Eq. (2) are shown in Tab. 1.

Material	$1.15\,\Delta K_{IIeff,th} \geq \Delta K_{Ieff,th}$	deflection a_{II}	mode mixity $\Delta k_{IIeff}/\Delta k_{Ieff}$
ARMCO iron	$1.7 < 2.7$	19°	1.88
Titanium	$2.0 \approx 2.0$	39°	0.71
Ferritic-pearlitic steel	$3.1 > 3.0$	50°	0.40
Nickel	$3.3 > 2.3$	52°	0.36
Pearlitic steel	$3.1 > 3.0$	60°	0.19
Stainless steel	$2.9 > 2.3$	67°	0.06

Table 2: Fulfillment of the mode I branching criterion and comparison with the real tendency to mode I crack growth measured on fracture surfaces of the six tested materials in terms of deflection angles a_{II} and local mode mixities according to Eq. (4).

SUMMARY

Effective thresholds and fracture surface morphology in 3D were measured for mode II and mode III cracks in the ferritic-pearlitic and the pure pearlitic steel. Both the deflection angle and the mode II threshold were much higher in the ferritic-pearlitic and pearlitic steels than in the ARMCO iron. After the local mode I growth was triggered in the pearlitic grain, the crack propagation continued with a large component of mode I also in the rest of the material. A criterion for mode I deflection from the mode II crack-tip loading, which uses values of the effective mode I and mode II thresholds, was in agreement with fractographical observations. It was not fulfilled in materials with low deflection angles from the maximum shear plane (ARMCO iron, titanium) and was fulfilled in materials with a high component of local mode I (nickel, ferritic-pearlitic, pearlitic and austenitic steels). In the ferritic-pearlitic and pearlitic steels, the reason for such behaviour was the presence of the secondary-phase particles (cementite lamellas), unlike in the previously austenitic steel, where the fcc structure and the low stacking fault energy were the main factors. Identification of the effect of microstructure of multiphase materials contributes to the research of shear-mode crack growth micromechanisms.

ACKNOWLEDGMENTS

The authors acknowledge the financial support of this work by the Czech Science Foundation in the frame of the project No. P108/12/0144 and by the European Regional Development Fund (CEITEC CZ.1.05/1.1.00/02.0068).

REFERENCES

[1] Vojtek, T., Pokluda, J., Hohenwarter, A., Pippan, R., Three-dimensional Morphology of Fracture Surfaces Generated by Modes II and III Fatigue Loading in Ferrite and Austenite, Engng Fract Mech, 108 (2013) 285-293.

[2] Vojtek, T., Pippan, R., Hohenwarter, A., Holáň, L., Pokluda, J., Near-threshold Propagation of Mode II and Mode III Fatigue Cracks in Ferrite and Austenite, Acta Mater, 61 (2013) 4625-4635.

[3] Pokluda, J., Pippan, R., Vojtek, T., Hohenwarter, A., Near-threshold Behaviour of Shear-mode Fatigue Cracks in Metallic Materials, Fatigue Fract Engng Mater Struct, 37 (2014) 232-254.
[4] Pook, L.P., Crack Paths, Wit Press, Southampton - Boston, (2002).
[5] Stampfl, J., Scherer, S., Gruber, M., Kolednik, O., Reconstruction of surface topographies by scanning electron microscopy for application in fracture research, Appl Phys A, 63 (1996) 341-346.
[6] Taylor, J.G., Warin, P.E., Watson, P., Metallographic aspects of fatigue in pearlitic structures, in: Taplin, D.M.R. (Ed.), Advances in Research on the Strength and Fracture of Materials: Fatigue, Vol. 2B, ICF4, Pergamon, Waterloo, (1977).
[7] Iacoviello, F., Di Cocco, V., Rossi, A., Cavallini, M., Fatigue crack tip damaging micromechanisms in pearlitic ductile cast irons, Fatigue Fract Engng Mater Struct, 38 (2015) 238-245.